




# Research on Mine Smoke Detection Technology Based on Multi-Feature Fusion Analysis

Xiankang Huang, Zuzhi Tian <sup>\*</sup>, Chusen Wang, Fangwei Xie and Jinjie Ji,  
School of Mechanical and Electrical Engineering, China University of  
Mining and Technology, Xuzhou 221000, China

**Received:** 9 January 2024/**Accepted:** 11 June 2024

**Abstract.** Traditional smoke detection sensors are characterized by low sensitivity, poor stability, etc. In this study, we propose a coal mine smoke detection technique based on multi-feature fusion analysis. Detection of smoke on belt conveyors is realized by machine vision technology. Firstly, the inter-frame difference method is used to capture the motion region of the smoke. And the suspected smoke region is obtained. Then, the color features of smoke are obtained by RGB color histogram. The motion direction features of smoke are obtained by smoke optical flow vector extraction. The irregular contour features of smoke are obtained by smoke contour irregularity criterion statistics. Based on obtaining the suspected smoke area, the above three features are used to determine whether the belt conveyor produces smoke. This study collected four video images of the belt surface smoke, stand smoke, light samples, and dust samples. The final combined diagnostic rate was 94.19% by testing the above detection models. This study proposes a stable and effective smoke detection technique for coal mine safety production.

**Keywords:** Smoke detection, Belt conveyor, Multi-feature fusion analysis, Machine vision, Color features

## 1. Introduction

With the improvement of automation level, coal production is growing rapidly [1]. But at the same time, safety accidents in coal mines frequently occur [2, 3]. Belt conveyor failure is one of the main causes of safety accidents in coal mines [4]. Common failures of belt conveyors include carrier roller failures, belt tears, and roller failures [5]. The carrier roller failures and the roller failures easily lead to the slipping phenomenon between the rolling body and the conveyor belt. The carrier roller failures and the roller failures easily lead to the slipping phenomenon between the rolling body and the conveyor belt. When the slipping failure occurs, there is a relative movement between the conveyor belt and the driving drum, which causes friction to generate heat. When the temperature rises to the ignition

---

\*Correspondence should be addressed to: Zuzhi Tian, E-mail: [tianzuzhi2023@163.com](mailto:tianzuzhi2023@163.com)



point of the conveyor belt material, it will ignite the conveyor belt and cause a fire. Due to the complex underground environment of coal mines and many combustible materials, once a fire occurs, the fire will spread rapidly [6]. There is even a possibility of a gas explosion due to the expansion of the fire. This poses a great threat to the life safety of underground workers.

Smoke is often produced before an open flame appears. Therefore, the detection of smoke can effectively achieve fire warning. Smoke sensors commonly used in underground mines generally use the principle of physical infrared or chemical changes to detect smoke [7]. De Rosa [8] evaluated the effectiveness of optical flame detectors, photoelectric smoke detectors, and combined ionization and photoelectric smoke detectors for rapidly detecting mining equipment cab fires. However, the bad underground environment can easily lead to sensor failure. Shi [9] trained the diagnostic system on fire and smoke images and assisted in determining fires with fire detectors and smoke detectors. But traditional smoke detection sensors have the characteristics of low sensitivity, small range, and poor stability. At present, machine vision technology is becoming more and more mature and is widely used in the field of fault detection.

Compared with the traditional smoke sensor, the visual method is more intuitive and the diagnosis rate is high. In addition, when the camera fails, it is easier to detect and replace it in time. The reliability is higher. Zhao [10] obtained fire data by infrared CCD. He then extracted the fire features and quantified them into a GA-improved wavelet neural network model. Finally, the detection of the fire is realized. Lee et al. [11] generated candidate smoke regions. Then he detected smoke based on fire-starting regions and predicted the direction of smoke movement. The reflection of coal dust and water vapor can lead to blurred images, low resolution, and obscured smoke contours. Wu et al. [12] proposed an image enhancement method based on dark primary color prior and CLAHE algorithm. The experimental results show that the images obtained by this algorithm have real, natural, and clear smoke contours. Kaabi et al. [13] conducted a comparative study of different methods for detecting smoke using image processing techniques and demonstrated each method's performance and detection rate. Feng et al. [14] proposed a new algorithm for smoke root detection. The algorithm synthesizes static and dynamic features of smoke and detects final smoke roots based on clustering and circles. The above algorithms are also based on machine vision to achieve smoke detection, but the above algorithms also have problems of low accuracy and poor stability. Lin [15] et al. developed a joint detection framework based on faster RCNN and 3D CNN. The detection rate of the smoke video sequence was 95.23%. Tao [16] et al. present two automatic smoke vehicle detection methods based on spatiotemporal bag-of-features (S-BoF) and professional convolutional neural network (P-CNN). The detection rate of the smoke video sequence was 91.07%. Zheng [17] et al. evaluated the effectiveness of several deep convolutional neural network algorithms in real-time detection of forest fire smoke, include the EfficientDet, Faster R-CNN, YOLOv3, SSD and advanced CNN model. The EfficientDet algorithm achieves an average detection accuracy of 95.7%. Although the accuracy of the CNN algorithm is high, it also has the problem that the training time is too long.

Based on the above smoke detection methods, this study proposes a coal mine underground smoke detection technique based on multi-feature fusion analysis. This study realizes the detection of smoke in belt conveyors based on machine vision technology. Firstly, the inter-frame difference method is used to capture the motion region of the smoke and obtain the suspected smoke region. Then the RGB color histogram obtains the color characteristics of the smoke. The smoke optical flow vector extraction obtains smoke motion direction features. The smoke contour irregularity criterion statistic is used to obtain the smoke irregular contour feature. On the basis of obtaining the suspected smoke area, the above three features are used to determine whether the belt conveyor produces smoke. This study is expected to collect four video images of the belt surface smoke, the stand smoke, light samples, and dust samples. The algorithm accuracy is then tested by the above detection model. Through the above detection algorithm model, we aim to obtain a stable and effective smoke detection technology to guarantee coal mine production safety. Through the above detection algorithm model, we innovatively apply machine vision to coal mine smoke alarms. We hope to obtain a stable and effective smoke detection technology to improve the safety of coal mine production.

## **2. Motion Area Detection**

When smoke appears in the underground tunnel of a coal mine, the smoke has obvious dynamic characteristics due to the influence of underground ventilation conditions. The camera shooting view is fixed. The alleyway environment can be used as the background. Then, the smoke is an obvious moving target. Therefore, if a moving target can be effectively detected downhole, it can be recognized as a suspected smoke area. The smoke can then be accurately detected based on a multi-feature fusion fault determination method.

(1) The inter-frame difference method.

The Inter-frame difference method utilizes two adjacent frames acquired by the camera for differencing [18]. Thus, the difference region between the two images is obtained. And the region of difference is the region of motion. The inter-frame difference method has less complexity of procedure and faster extraction speed. The principle is shown in Equation (1):

$$F_i(x, y) = |f_i(x, y) - f_{i-1}(x, y)|, \quad (1)$$

where:  $f_i(x, y)$  and  $f_{i-1}(x, y)$  are two neighboring frames in the acquired image sequence.  $F_i(x, y)$  is the inter-frame difference obtained by differencing two frames of image.  $(x, y)$  are the coordinates of the pixels in the image.

When the inter-frame difference method is used in the actual environment of underground coal mines, there are also slight differences in the background within the two frames due to illumination, reflections, etc. Therefore, the binary method was used to process the difference result images in this study. Even if there is a background in the difference result, the regional pixel intensity is low. Therefore,

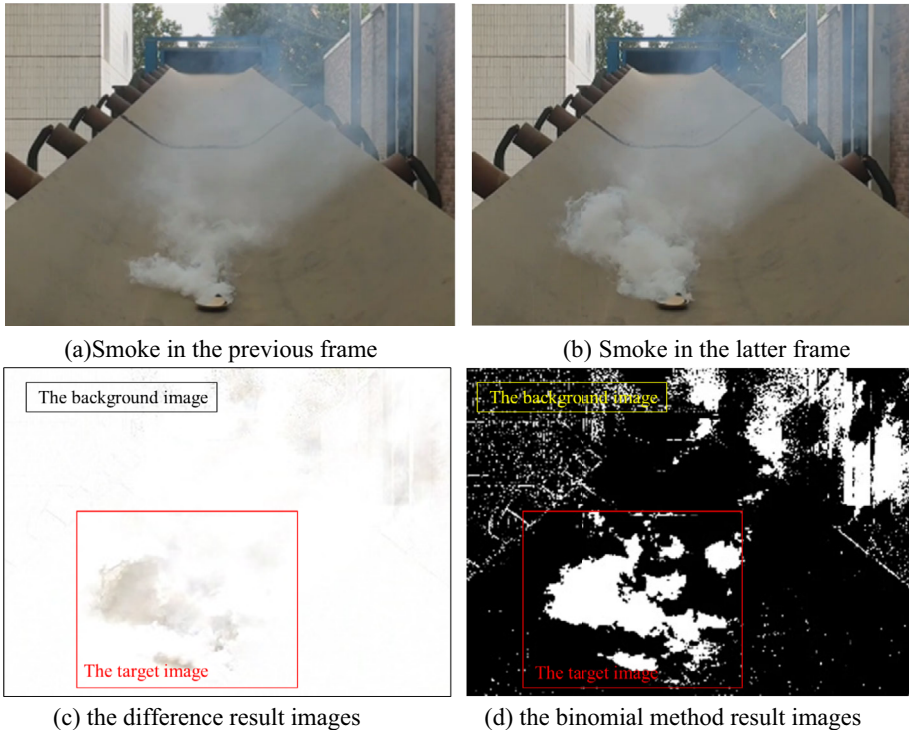


**Figure 1. Interframe differential detection of smoke images.**

it is only necessary to set a suitable threshold value  $T$ . Pixels with intensity greater than the threshold value are determined as the target pixels, and those below the threshold value are determined as background pixels. This effectively removes interfering areas and preserves the target image. The principle of the binomial method is shown in Equation (2):

$$R_i(x, y) = \begin{cases} 0, & F_i(x, y) < T \\ 1, & F_i(x, y) \geq T \end{cases} \quad (2)$$

The simulated smoke image is processed using the inter-frame difference method and the binary method to extract the different regions of two neighboring frames, and the effect is shown in Figure 1.

Figure 1a and b are the smoke images of two adjacent frames. Figure 1c is the extracted difference image. Figure 1d is the result of the binary method. As shown Figure 1d, The background image is still obvious and needs further processing.

(2) Open arithmetic operation.

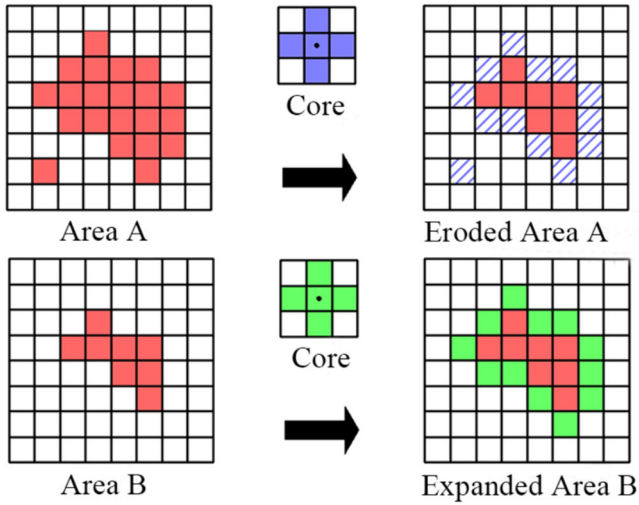


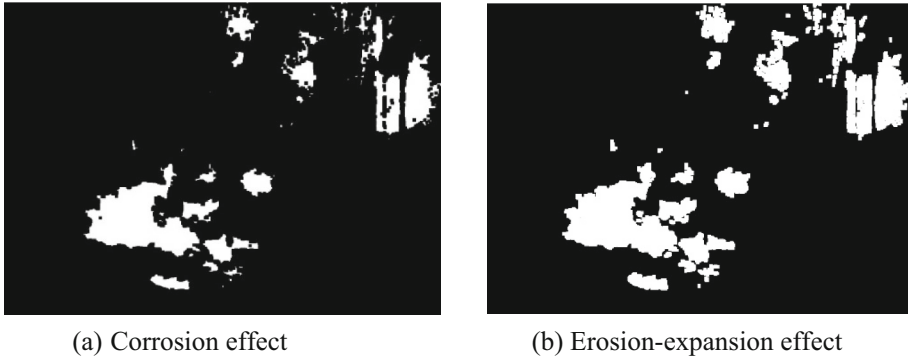
**Figure 2. Corrosion and expansion operation schematic.**

Open arithmetic operation is a treatment in the order of erosion-expansion [19]. Erosion and expansion are operations that convolve an image with a kernel. This enables the reduction and enlargement of highlighted regions. The principle of corrosion and expansion operation is shown in Figure 2.

As shown in Figure 2. The process of the erosion operation is to overlap the kernel with region A. While keeping region A completely wrapped around the nucleus, the pixels that can pass through the origin of the nucleus are kept at this point. The rest of the pixels were removed. The expansion operation process keeps the origin of the kernel contained in region B. All pixels that the kernel can expand are expanded pixels.

The processing in the order of erosion-expansion is an open arithmetic operation. This can be used to eliminate small highlighted pixels. The processing in the order of expansion-erosion is a closed arithmetic operation. And this can be used to eliminate small cavities. There are many interfering pixels in Figure 1d. So, the open arithmetic operation is applied to them. The processing results are shown in Figure 3.

The result after open arithmetic processing is shown in Figure 3b. The background interfering pixels were obviously eliminated. The extraction of the moving target was accomplished. The inter-frame difference method utilizes two adjacent frames to make a difference. This can lead to severe nulling of the detected target when the moving target is moving faster. If the hole is small, the closed arithmetic operation will eliminate the hole. The illustrated voids are large, and the use of closed arithmetic operations would result in distortion of the overall shape of the region. Therefore, the closed arithmetic operation is not performed in this paper.



(a) Corrosion effect

(b) Erosion-expansion effect

**Figure 3. Open operation results of smoke image.**

### 3. Auxiliary Judgment Feature Extraction

After completing the motion area capture, the motion area is the suspected smoke area. However, it is not possible to determine that is the smoke area based on this. Further judgment is required in conjunction with the characterization of the smoke. When mining operations are carried out underground in coal mines, mining dust and harmful gases need to be ventilated. And the underground tunnel space is narrow. Thus, the smoke has different characteristics when it appears underground in coal mines than in open environments. The features of coal mine underground smoke can be extracted and analyzed to improve the accuracy of smoke determination.

#### 3.1. Color Features

The color feature is the most significant static feature. Distinct color features exist in smoke. And large differences between the smoke area and the background [20, 21]. Everyday visible colors are made by mixing the three primary colors of red, blue, and green light in different proportions. The colors all conform to the distribution of the coordinate system shown in Figure 4. All colors have a coordinate point corresponding to the square space shown in the figure. Due to the distinctive color characteristics of smoke, the RGB model coordinate points corresponding to its color will only change in a fixed area.

This part is used to reflect the target region's color characteristics by extracting the region's RGB three-channel components. In order to accurately analyze the color characteristics of smoke, pictures of dust and downhole lights were selected for comparison. It is used to accurately analyze the difference between smoke, dust, and light. As shown in Figure 5.

As shown in Figure 5, the interference factors, such as the background environment in the image, are very serious. The area where the study object is located is selected to make the extracted color features more visible. To make the extracted color features more visible, the study object area is selected. And the color fea-

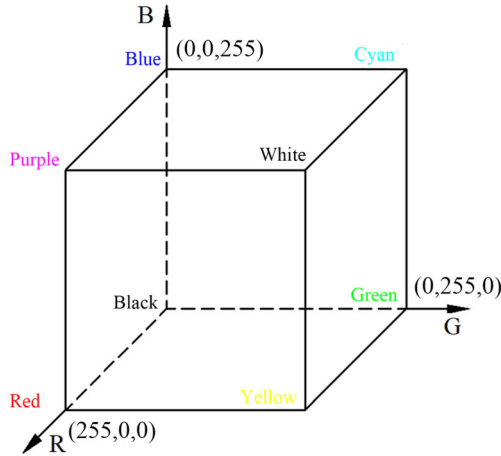


**Figure 4. RGB coordinate distribution model.**

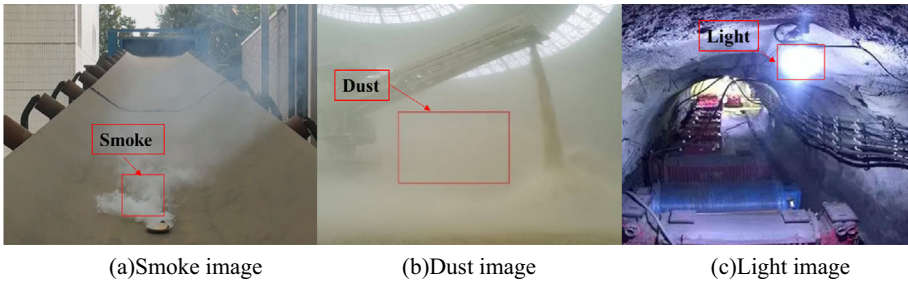
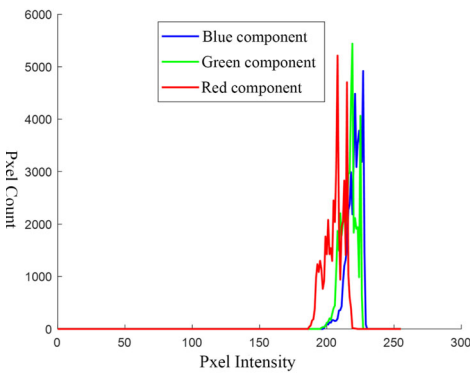


**Figure 5. Compared images of different environments.**

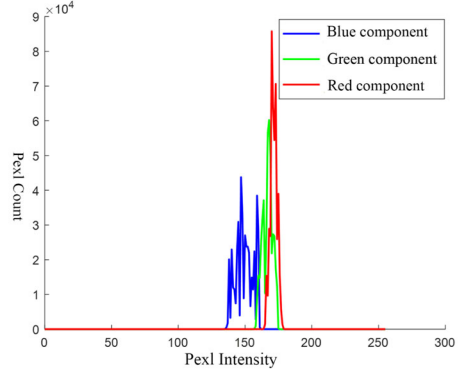
tures are extracted. The extraction results of the RGB three-channel histogram for the selected region in Figure 5 are shown in Figure 6.

Compare the smoke histogram with the dust and light histogram. In the smoke histogram, the three-channel components have similar rules, and are distributed in the higher intensity pixel interval. In the dust histogram, the blue and green channel components are distributed in the medium intensity region, and the three-channel components are not similar. In the histogram of light, the three-channel component increases slowly, and the distribution law is different from that of smoke and dust.

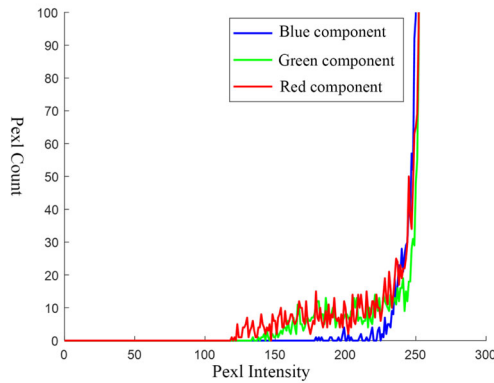
By analyzing the histograms, it can be seen that smoke differs significantly from dust and light in terms of color features. So, the color feature can be used as a method to assist in determining smoke faults.



(a) Smoke histogram



(b) Dust histogram



(c) Light histogram

**Figure 6. RGB histogram of the selected region in the compared image.**

### 3.2. Motion Direction Features

In the coal mine tunnel, when there is smoke, the smoke will first move upward and then move to the side of the wind. The analysis of the smoke movement feature of continuous frames of video is helpful in identifying the underground smoke accurately [22, 23].

Figure 7 shows two frames taken from the smoke video. In order to simulate the underground conditions of a coal mine, a unidirectional wind of a certain velocity was applied to the smoke so that it moved in the direction of the airflow.

The optical flow method is a method of determining the motion information of the observed target based on the difference in object position between neighboring frames of the video. This method can be used to analyze the motion of the observed target relative to the observer. It can also record the instantaneous





(a)Smoke in the previous frame

(b) Smoke in the latter frame

**Figure 7. Smoke dispersion in a simulated environment.**

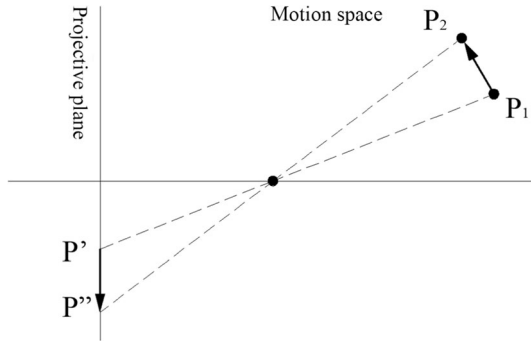


**Figure 8. Projection of the sports field.**

velocity and displacement of moving objects in space for a set period. The optical flow field of an object in motion is obtained by projecting the object in three dimensions onto a two-dimensional plane. The optical flow field can show the motion of the observed target. The schematic diagram is shown in Figure 8.

In a three-dimensional projection, the optical flow moves from  $P_1(x_1, y_1)$  to  $P_2(x_2, y_2)$ , and the projection point moves from  $P'(x_3, y_3)$  to  $P''(x_4, y_4)$ . Then, the length of the optical flow vector is shown in Equation (3).

$$d = \sqrt{(x_2 - x_1)^2 + (y_2 - y_1)^2} \quad (3)$$

The phase angle of the optical flow vector is shown in Equation (4):

$$\theta = \arctan \frac{y_2 - y_1}{x_2 - x_1} \quad (4)$$

The projected distance in a two-dimensional plane is:

$$D = d * \cos \theta \quad (5)$$



**Figure 9. Optical flow vector of smoke extraction.**

The optical flow method is utilized to extract the optical flow vectors from the simulated mine smoke video. The results are shown in Figure 9.

In order to make the optical flow vectors detected by the optical flow method clearer, the optical flow vectors with vector lengths greater than or equal to the set threshold are retained for smoke motion detection in the image shown in Figure 9. The optical flow vector contains motion information. By analyzing the direction of the optical flow vector, we can obtain the smoke's movement direction law in the coal mine's ventilation state underground. As shown in Figure 9, the direction of spatial motion is divided into eight phases at  $45^\circ$  intervals. And the number of optical flow vectors within the eight-phase intervals is counted. As shown in Figure 10.

To minimize the effect of background information, only optical flow vectors with vector lengths greater than or equal to the set threshold are retained in the statistics. The length threshold of the optical flow vector at the smoke feature point is set to  $d = 1 \times 10^{-2}$ . The statistical results of the directional distribution of the motion optical flow for different frames selected from the smoke video are shown in Figure 11.

Figure 11 shows the results of the optical flow direction obtained from the statistics of frames 5, 10, 15, and 20 in the smoke video, respectively. It can be seen that the direction of the optical flow vectors in the first three statistics lies more in phase intervals 1 to 4 and less in the rest of the phase intervals. This is consistent with the characteristics of the upward motion of the smoke. The results of the fourth count do not conform to the above pattern. This can be attributed to the fact that when the video was shot, the smoke moved closer to the camera due to the influence of opposing winds. Combined with the actual conditions of coal mine underground, the rising direction and ventilation direction can be defined as the main movement direction. This feature can be used as a supplementary method to further detect the suspected smoke area.

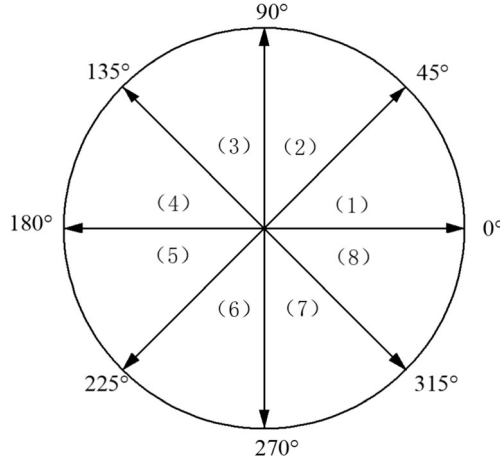


**Figure 10. Division of spatial motion direction.**

### 3.3. Contour Features

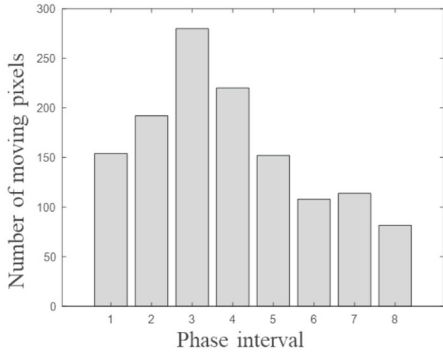
Smoke has a unique contour compared to the background targets that can be observed underground in coal mines. Its shape is fluid and changing all the time [24, 25]. Therefore, in this study, the contour feature is selected as one of the auxiliary features for determining smoke faults. In this part, the smoke contour is extracted using the binary method, and then the extraction results are processed by the open operation to obtain the smoke shape. The detection results are shown in Figure 12.

Generally, when two figures are equal in area, an irregular figure's perimeter is greater than a regular figure's. As shown in Figure 12, the result of open operation shows that the smoke contour is irregular. Therefore, the contour of the graph is extracted by the Canny edge detection method. The ratio is done with the contour length of the outer rectangle of the region. This ratio can be used as a basis for the determination of suspected smog areas. The Canny edge detection results and the outer rectangle are shown in Figure 13.

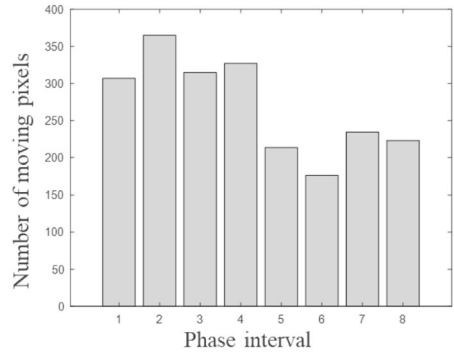
The contour irregularity criterion is shown in Equation (6):

$$cirt = \frac{obj}{con}, \quad (6)$$

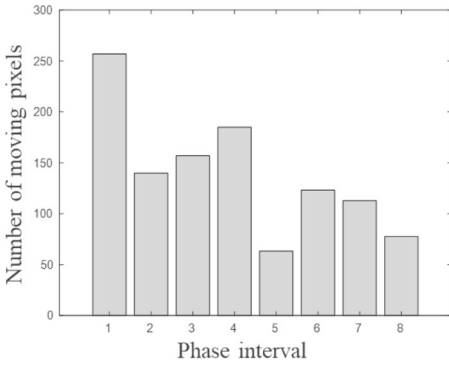
where *obj* is the contour length of the smoke obtained by edge detection, its unit is a pixel. As shown by the black contour line in Figure 13a, *con* is the perimeter of the smallest outer rectangle of the contour line. Its unit is a pixel. As shown by the red line in Figure 13b, *cirt* is the determination basis of the irregular shapes. The *cirt* values were calculated and counted for the simulated smoke video sequences. And the trends were plotted as shown in Figure 14.



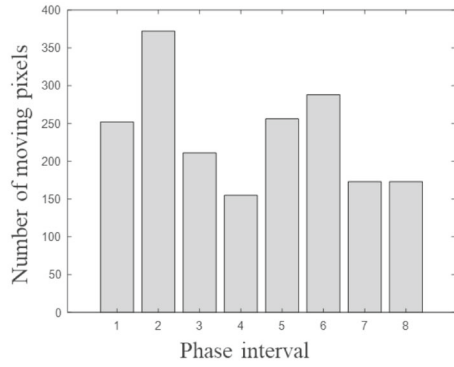
(a) Frame 5



(b) Frame 10



(c) Frame 15



(d) Frame 20

**Figure 11. Statistics of optical flow direction distribution.**



(a) Smoke image

(b) binary image

(c) open operation image

**Figure 12. Detection of smoke shape characteristics.**

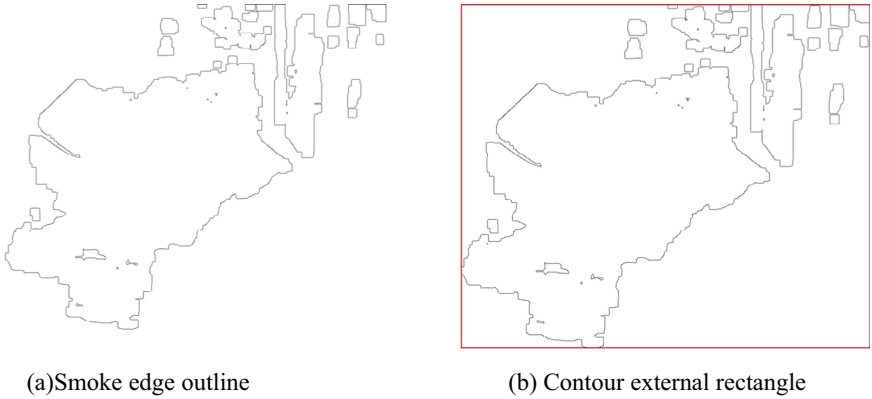


**Figure 13. Smoke region contour extraction.**

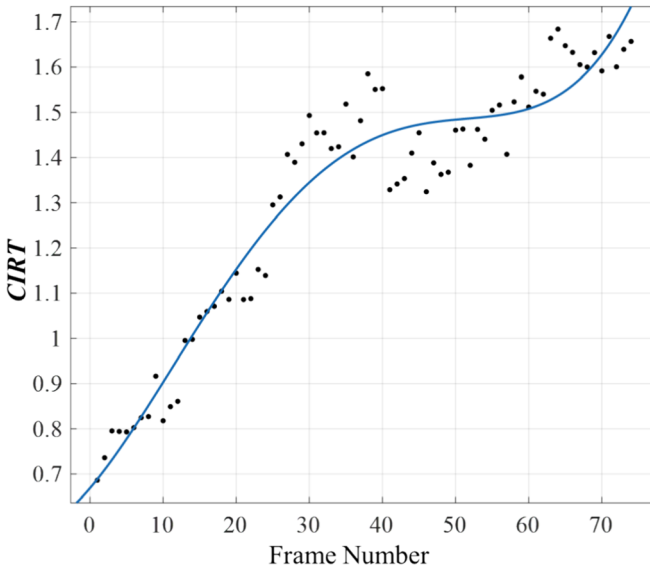


**Figure 14. Statistics of contour irregularity criterion of simulated smoke.**

As seen in Figure 14, the value of the irregularity determination of the smoke contour tends to increase with the change of time. And the rate of growth is changing from fast to slow. This characteristic can be used as one of the auxiliary bases for smoke detection.

## 4. Multi-feature Fusion Analysis

The color features, motion direction features, and contour features of the suspected smoke region were extracted in the previous section. Determining factors and rules based on the patterns that exist in the three different characteristics of coal mine smoke. Smoke is recognized when all the criteria set are met.

### 4.1. Color Features Analysis

In the previous section, the RGB three-channel components of the smoke image were extracted, as shown in Figure 6a. The RGB three-channel components of the smoke have a similar distribution pattern and are all distributed in the pixel interval of higher intensity. Set the color feature judgment factor as shown in Equation 7:

$$\begin{cases} C_{\min} = \min(R, G, B) \\ C_{\max} = \max(R, G, B) \\ I = (R + G + B)/3 \end{cases} \quad (7)$$

Based on the three judgment factors shown in Equation (7), the following three decision rules (8) are given:

$$\begin{cases} |C_{\max} - C_{\min}| < t \\ L_1 < I < L_2 \\ D_1 < I < D_2 \end{cases}, \quad (8)$$

where:  $t$  is the interval length threshold set according to the smoke characteristics,  $L_1$  and  $L_2$  are the upper and lower thresholds under better lighting intensity conditions, and  $D_1$  and  $D_2$  are the upper and lower thresholds under poorer lighting conditions. According to the smoke RGB component map shown in Figure 6. Considering a certain fault-tolerant space. Set:  $t = 40$ ,  $L_1 = 170$ ,  $L_2 = 230$ ,  $D_1 = 110$ ,  $D_2 = 170$ .

When the smoke feature satisfies the decision rule 1 and rule 2 in Equation (8) at the same time or satisfies the decision rule 1 and rule 3 in Equation (8) at the same time, it is judged to satisfy the color feature of smoke.

### 4.2. Motion Direction Analysis

Based on the extraction and analysis of optical flow vectors of the simulated mine smoke. It can be seen that when the smoke is generated, the direction of the smoke motion in addition to meeting the characteristics of the rise. Ventilation of the environment also has a certain relationship. Therefore, a main direction of motion can be determined based on the mine ventilation. In most cases, the motion vector of the smoke is greater than 50% in the main direction of motion. Combining the results of the analysis in chapter 3.2, the spatial orientation can be divided into the four regions shown in Figure 15. Based on the characteristics of underground ventilation and smoke rise, area (1) is identified as the main direc-

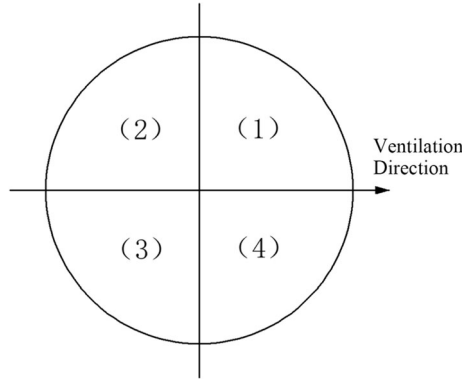


**Figure 15. Division of space direction during underground ventilation.**

tion of movement. However, there is a shape change of the smoke during the motion, which may lead to the reversal of the optical flow. Therefore, region (3) is considered in the main direction of motion as well.

The direction of the moving optical flow vectors of the smoke is counted as a judgment factor for the directional characteristics of the smoke, as shown in Equation (9):

$$A_i = \text{sum} \left[ \frac{\pi}{2}(i-1) < P_\theta < \frac{\pi}{2}i \right], i = 1, 2, 3, 4 \quad (9)$$

Based on the judgment factors shown in Equation (9), the following decision rule (10) is given:

$$A_{\text{main}} > 0.5A_{\text{all}}, \quad (10)$$

where:  $A_{\text{main}}$  is the number of optical flow vectors in the main motion direction.  $A_{\text{all}}$  is the total number of optical flow vectors greater than a set length threshold. When the number of optical flow vectors in the main direction of motion is more than 50% of the total number of optical flows, it is judged to satisfy the motion direction characteristic of smoke.

### 4.3. Contours Change Features Analysis

As can be seen from the results of the irregular criterion statistics shown in Figure 14. The irregularity criterion  $CIRT$  tends to increase when the smoke undergoes diffusion motion. However, the increase in  $CIRT$  is not monotonically increasing but fluctuates significantly after increasing to a certain level. Therefore,  $CIRT$  is grouped to take the mean value. And the data were divided into 18 groups in this study. The trend of the mean value  $CIRT$  is analyzed as a judgment of the change rule of shape. As shown in Figure 16.

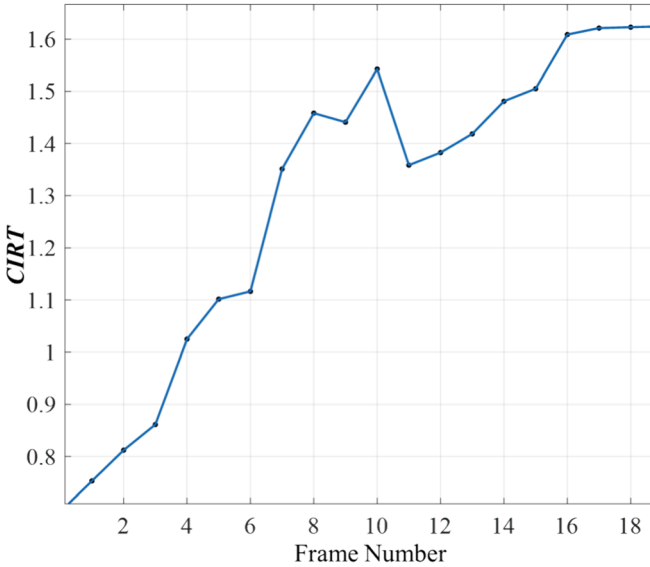


**Figure 16. Variation trend of the mean value of contour irregularity criterion.**

As seen from the change in the folded line in Figure 15, the *CIRT* monotonically increases when the smoke first begins to diffuse. When smoke spreads to a certain level, *CIRT* fluctuates. Therefore, the decision condition is satisfied when there is a clear succession of multiple increments. In this study, *CIRT* value was used as a judgment factor as shown in Equation (11):

$$CIRT_i = \frac{cirt_{4i-3} + cirt_{4i-2} + cirt_{4i-1} + cirt_{4i}}{4} \tag{11}$$

Based on the judgment factors shown in Equation (11), the following decision rule (12) is given:

$$CIRT_i \leq CIRT_{i+1} \tag{12}$$

When a moving region is detected, a continuous shape criterion *CRIT* is extracted for the moving region. When the number of times satisfying formula (12) is greater than or equal to 15, it can be determined that the contours change features are satisfied.

#### 4.4. Smoke Detection

The color features, motion direction features, and contour features extracted in this study are used as the basis for smoke detection. It has the characteristics of real-time, fast calculation speed, and high reliability in video monitoring. When some frames of the image do not meet the criteria, it can also not affect the over-



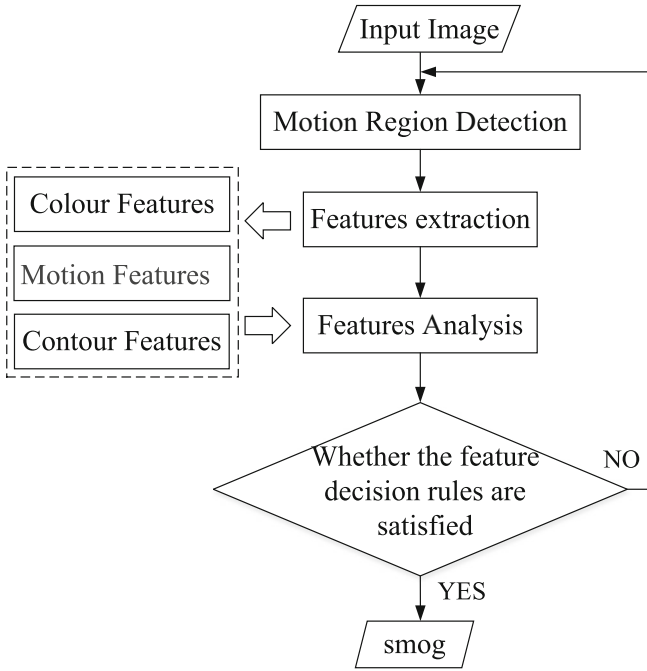


**Figure 17. Flowchart of smoke detection.**

all recognition effect. Based on the previous research, the smoke detection flow chart shown in Figure 17 is summarized.

In Figure 17, the motion region detection is the preliminary detection of the suspected region. The fixed background region is removed to reduce the calculation amount. Feature extraction is to extract the color features, motion features, and contour features of the suspected area. In the step of feature analysis, the corresponding rules are determined to determine whether it is smoke. According to the above processing steps, the smoke video used in the previous analysis is selected for testing, and the test effect is shown in Figure 18.

Figure 18a–c are the images of artificial smoke on the conveyor belt surface. The actual smoke area is large. And the smoke concentration is low in some areas. The algorithm only detects the area with a large concentration. Because the background is brighter in the lower concentration area of smoke. No obvious motion and shape features of smoke are observed in this area. Therefore, the determination effect in this area is poor, but it can still ensure the detection effect of smoke.

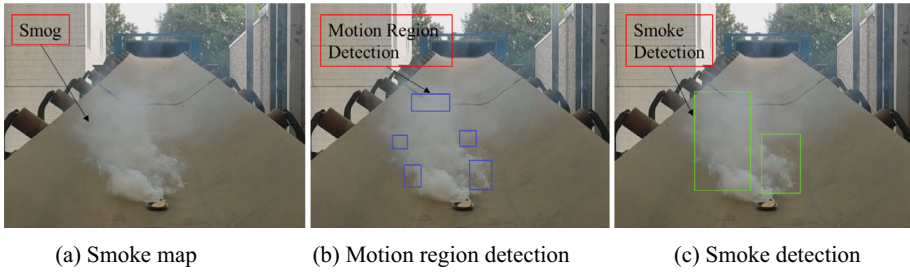


**Figure 18. Smoke detection test.**

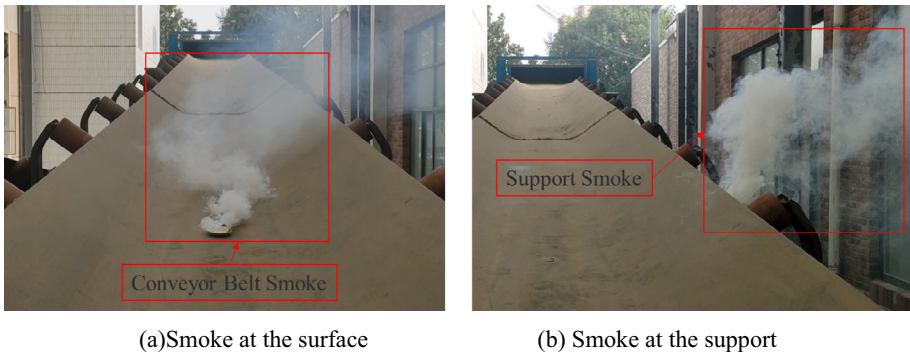


**Figure 19. Positive sample video images with smoke.**

## 5. Results and Discussion

In this study, two different smoke videos were selected as positive samples. The artificial smoke is produced at the belt surface and support of the belt conveyor. And the numbers are Video1 and Video2, as shown in Figure 19.

To verify the false positive probability of the detection algorithm proposed in this study. Considering the possible interference factors in the coal mine, interference videos containing flashlight light and dust are selected, respectively. The numbers are Video3 and Video4, as shown in Figure 20. As in Figure 20a, there is an illuminated light on the right wall. And in Figure 20b, there is flying dust. This component was chosen as a negative sample factor to test the false positives and accuracy of the algorithm.

The frame rates of the above four test videos are all 30fps. Based on the above smoke detection algorithm, the experimental detection results are shown in Table 1.

From the data in the table, it can be seen that the detection accuracy of the positive sample Video1 is higher. And the accuracy can reach 95.04%. In contrast, the positive sample Video2 was detected with lower accuracy. It was 89.63%. This may be due to the fact that the belt conveyor was in an environment with oppos-

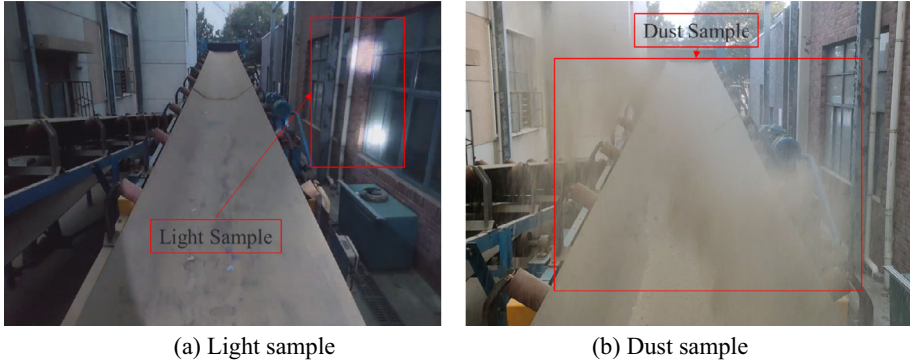


**Figure 20. Negative sample video images with interference factors.**

**Table 1  
Test Results of Experimental Video Samples**

Video sample sequence number	Video frame count	Alarm frame count	Correct frame count	Accuracy rate (%)
Positive sample	Video1	1068	1015	95.04
	Video2	1186	1063	89.63
Negative sample	Video3	709	31	95.63
	Video4	649	23	96.46

ing winds when the video shoot was conducted. The direction of the smoke motion to the lower right of the belt changes with the direction of the wind, which can lead to changes in the motion characteristics of the smoke. Whereas in Video1, the smoke is above the belt and is less affected by the opposing winds. Negative samples Video3 and negative samples Video4 both have high accuracies. The color characteristics of the light as a distraction differ significantly from the smoke. RGB three-channel components are located in a zone higher than the smoke image. At the same time, the shape of the light is relatively regular and fixed, which does not satisfy the basis for determining the irregularity of the shape of the smoke. The dust video shows man-made dust being thrown. The direction of motion is predominantly diagonal downward, which distinguishes it from the diagonal upward motion characteristic of smoke. Moreover, the color characteristics of dust are also more distinct from smoke. Therefore, both Video3 and Video4 have a high degree of accuracy. After obtaining the smoke video, the average reasoning speed of the smoke is 120 fps, which is enough to meet the requirements of underground use in coal mines.

In order to visualize the degree of accuracy of the proposed algorithm in this study, the combined Accuracy Rate was chosen as the evaluation metric. The formula is shown below:

$$AR = \frac{TP + FN}{TP + TN + FP + FN} \times 100\%, \quad (13)$$

where:  $TP$  is the probability of detecting smoke in the presence of smoke;  $TN$  is the probability of detecting smoke in the absence of smoke;  $FP$  is the probability of detecting no smoke in the presence of smoke; and  $FN$  is the probability of detecting no smoke in the absence of smoke.

$TP$  and  $FP$  sum to 1 for positive samples.  $TN$  and  $FN$  sum to 1 for negative samples. Since the experiment used two positive and two negative samples, the combined accuracy needs to be divided by 2. Bringing in the test data in Table 1 into Equation (13). It can be obtained (14):

$$AR = \frac{95.04\% + 89.63\% + 95.63\% + 96.46\%}{2 \times 2} \times 100\% = 94.19\% \quad (14)$$

The smoke detection algorithm proposed in this study has a high accuracy. The comprehensive accuracy of 4 positive and negative samples can reach 94.19%. Because of the existence of negative samples, it shows that the algorithm has strong anti-interference ability.

## 6. Conclusion

Detection of smoke on belt conveyors is realized by machine vision technology. This study proposed a coal mine smoke detection technique based on multi-feature fusion analysis. Color features, motion direction features, and contour features have been extracted for the suspected smoke area. The detection of smoke is completed based on the above features. The combined accuracy of the final test was 94.19%. This method solves the problem of small range and low stability of traditional smoke sensors. Compared to the existing algorithms based on visual diagnostic smoke, the model is lighter and more accurate. Aiming at the problem of the harsh environment in the coal mine, the equipment is easy to be damaged. Although the vision-based diagnostic method does not solve the problem of easily damaged equipment, the method makes it easier to detect equipment damage and make timely treatment. The method proposed in this study is characterized by high accuracy, high reliability, and real-time detection. The above confirms the feasibility of this method for underground smoke detection, which is of great significance for preventing underground fires and maintaining safe production in coal mines.

In terms of coal production, cameras can be arranged on the mining face, which can monitor the mining situation in real time and detect whether smoke is produced through smoke detection technology to prevent fire. In terms of coal transportation, belt conveyors are widely used in underground main transportation, such as the coal face transportation roadway, coal transportation gallery, coal transportation trestle, and so on. Surveillance cameras can be arranged above the belt holder to monitor the coal transportation situation and whether smoke is

## *Research on Mine Smoke Detection Technology Based on Multi-Feature Fusion Analysis*

produced in real-time. Smoke detection technology can also be used in areas prone to fire, such as forest fire monitoring and building fire monitoring. Further research in this area can be increased.

### **Acknowledgements**

This research was supported by the National Natural Science Foundation of China (52005426, 52375069, 52305078), Major Basic Research Project of the Natural Science Foundation of the Jiangsu Higher Education Institutions (22KJA460013).

### **Data Availability**

The datasets generated during and/or analysed during the current study are not publicly available due to privacy, but are available from the corresponding author on reasonable request.

### **Declarations**

**Conflict of interest** The author(s) declared no potential conflicts of interest with respect to the research, authorship, and/or publication of this article.

### **SUPPLEMENTARY INFORMATION**

The online version contains supplementary material available at <https://doi.org/10.1007/s10694-024-01602-z>.

### **References**

1. Wang XQ, Long SS, Meng XR (2022) Simulation and optimization of mining-separating-backfilling integrated coal mine production logistics system. *Energ Explor Exploit* 40:908–925
2. Wu B, Wang JX, Qu BL, Qi PY, Meng Y (2023) Development, effectiveness, and deficiency of China's coal mine safety supervision system. *Resour Policy* 82:103524
3. Wang YX, Fu G, Lyu Q, Wu YL, Jia QS, Yang XY et al (2022) Reform and development of coal mine safety in China: an analysis from government supervision, technical equipment, and miner education. *Resour Policy* 77:102777
4. Homisin J, Grega R, Kassay P, Fedorko G, Molnar V (2019) Removal of systematic failure of belt conveyor drive by reducing vibrations. *Eng Fail Anal* 99:192–202
5. Fedorko G (2021) Application possibilities of virtual reality in failure analysis of conveyor belts. *Eng Fail Anal* 128:105615

6. Wang JT, Wang FS, Xu YY, Dong XW (2019) Study on current situation and development trend for coal mine fire prevention technology in China. *Fresen Environ Bull* 28:5010–5016
7. Mokhtari Z, Hole S, Lewiner J (2013) Study of an ionic smoke sensor. *Meas Sci Technol* 24:055006
8. De Rosa MI, Litton CD (2010) Rapid detection and suppression of mining equipment cab fires. *Fire Technol* 46:425–435
9. Shi F, Qian HM, Chen W, Huang M, Wan ZC (2020) A fire monitoring and alarm system based on with OHEM. *Chin Contr Conf* . <https://doi.org/10.23919/CCC50068.2020.9189667>
10. Zhao H (2012) Research on fire detection in coal mine based on GA-improved wavelet neural networks. *Adv Mater Res-Switz* 490–495:1636–1639
11. Lee SJP, Son C, Paik J (2019) Smoke detection based on fire-starting regions. *IEIE Trans Smart Proc Comput* 8:475–481
12. Wu DM, Zhang SQ.(2018) Research on image enhancement algorithm of coal mine dust. 2018 International conference on sensor networks and signal processing, pp.261–265
13. Kaabi R, Frizzi S, Bouchouicha M, Fnaiech F, Moreau E. (2017) Video Smoke Detection Review State of the art of smoke detection in visible and IR range. 2017 International Conference on Smart, Monitored and Controlled Cities (Sm2c). pp.81–86
14. Feng XH, Cheng PL, Chen F, Huang Y (2022) Full-scale fire smoke root detection based on connected particles. *Sensors-Basel* 22:6748
15. Lin GH, Zhang YM, Xu G, Zhang QX (2019) Smoke detection on video sequences using 3D convolutional neural networks. *Fire Technol* 55:1827–1847
16. Tao HJ, Lu XB (2020) Smoke vehicle detection based on spatiotemporal bag-of-features and professional convolutional neural network. *IEEE Trans Circ Syst Vid* 30:3301–3316
17. Zheng X, Chen F, Lou LM, Cheng PL, Huang Y (2022) Real-time detection of full-scale forest fire smoke based on deep convolution neural network. *Remote Sens-Basel* 14:536
18. Li M, Wang Z, Ren JC, Sun MJ (2022) MVVA-net: a video aesthetic quality assessment network with cognitive fusion of multi-type feature-based strong generalization. *Cogn Comput* 14:1435–1445
19. Sun ZY, Sha AM, Zhang HL, Yao QL (2007) Study on the feature extraction technology of the asphalt mix image based on mathematical morphology. *Proc Int Conf Health Monitor Struct Mater Environ* 1:1178
20. Ye MQ, Luo YM (2023) A deep convolution neural network fusing of color feature and spatio-temporal feature for smoke detection. *Multimed Tools Appl* . <https://doi.org/10.1007/s11042-023-16495-3>
21. Tao HJ, Lu XB (2020) Smoke vehicle detection based on multi-feature fusion and hidden Markov model. *J Real-Time Image Proc* 17:745–758
22. Wu XH, Lu XB, Leung H (2018) A video based fire smoke detection using robust ada-boost. *Sensors-Basel* 18:3780
23. Qing L, Zhang XH, Na L (2011) Algorithm research on main motion direction feature extraction for initial rising smoke. *Appl Mech Mater* 58–60:495–500
24. Yin YF, Cheng H, Liu H (2020) Flue gas layer feature segmentation based on multi-channel pixel adaptive. *Multimed Tools Appl* 79:29069–29085

*Research on Mine Smoke Detection Technology Based on Multi-Feature Fusion Analysis*

25. Wang L, Li AG (2017) Early fire recognition based on multi-feature fusion of video smoke. Proc 36th Chin Control Conf . <https://doi.org/10.23919/ChiCC.2017.8028197>

**Publisher's Note** Springer Nature remains neutral with regard to jurisdictional claims in published maps and institutional affiliations.

Springer Nature or its licensor (e.g. a society or other partner) holds exclusive rights to this article under a publishing agreement with the author(s) or other rightsholder(s); author self-archiving of the accepted manuscript version of this article is solely governed by the terms of such publishing agreement and applicable law.